*Inorg. Chem.* **2003**, *42*, 2938–2949


# Aminomethyl-bipyridine Bearing Two Flexible Nitronyl-nitroxide Arms: A New Podand for Complexation of Transition Metals in a Facial or Meridional Conformation

**Christophe Stroh,[†] Elie Belorizky,[‡] Philippe Turek,[§] Hélène Bolvin,[||] and Raymond Ziessel*,[†]**

*Laboratoire de Chimie Moléculaire, Ecole de Chimie, Polymères et Matériaux (ECPM), UMR 7008, Université Louis Pasteur (ULP), 25, rue Becquerel, F-67087 Strasbourg Cedex 2, France, Laboratoire de Spectrométrie Physique, Université Joseph Fourier Grenoble 1, UMR 5588, B. P. 87, F-38402 Saint Martin d'Hères Cedex, France, Institut Charles Sadron, Université Louis Pasteur (ULP), 6, rue Boussingault, F-67083 Strasbourg Cedex, France, and Laboratoire de Chimie Quantique, Institut Le Bel, 4, rue Blaise Pascal, F-67000 Strasbourg, France*

Received July 29, 2002

Transition metal complexes of 6-aminomethyl-bis[methyl-2-(4,5-dihydro-4,4,5,5- tetramethylimidazolinyl-3-oxide-l-oxy)]-2,2′-bipyridine, bpyN(NIT)$_2$, **1**, have been synthesized and characterized by FAB-MS, UV–vis, FT-IR, and EPR spectroscopies, elemental analysis, and susceptibility measurements. Single-crystal X-ray diffraction studies have been performed on all compounds giving the following crystal data: bpyN(NIT)$_2$, **1**, triclinic, $P\bar{1}$, $Z = 2$, $a = 10.7224(4)$ Å, $b = 11.0995(4)$ Å, $c = 13.1134(3)$ Å, $\alpha = 114.101(9)°$, $\beta = 97.476(9)°$, $\gamma = 99.667(9)°$; ZnbpyN-(NIT)$_2$, **2**, hexagonal, $P3_2$, $Z = 3$, $a = 15.4545(3)$ Å, $b = 15.4545(3)$ Å, $c = 13.5594(3)$ Å; NibpyN(NIT)$_2$, **3**, hexagonal, $P3_2$, $Z = 3$, $a = 15.2867(1)$ Å, $b = 15.2867(1)$ Å, $c = 13.7160(1)$ Å; CubpyN(NIT)$_2$, **4**, triclinic, $P\bar{1}$, $Z = 2$, $a = 11.8640(4)$ Å, $b = 13.2023(4)$ Å, $c = 13.2661(5)$ Å, $\alpha = 90.539(9)°$, $\beta = 104.983(9)°$, $\gamma = 113.252-(9)°$. The two radicals of the free ligand **1** are almost perpendicular to one another in the solid state, favoring a weak ferromagnetic interaction ($J/k_B = 8.8$ K). The complexes obtained by wrapping the ligand around a single metal center gave rise to two different coordination schemes where the two radicals of **1** adopt a ON(3)O meridional (with Ni and Zn) or a ON(3)O facial conformation (with Cu), which strongly affects the magnetic and electronic properties (O accounts for the coordinated oxygen atoms of the nitroxide radicals and N(3) accounts for the tertiary amine). For **2**, a model of a dimer has been used giving rise to a weak antiferromagnetic interaction between the radicals ($J/k_B = -5.3$ K). For **3**, a very strong intramolecular antiferromagnetic coupling has been found and estimated at $J/k_B = -230$ K and $J'/k_B = -110$ K between the nickel and each radical using an asymmetric model of a trimer. For **4**, an unusual magnetic behavior is observed, dominated by antiferromagnetic interactions with a residual plateau at $\chi T = 0.63$ emu·K·mol$^{-1}$. Molecular modeling at the CASSCF level is in keeping with an antiferromagnetic coupling of the radical bound with the Cu(II) in the equatorial position. The combined structural, electronic, and magnetic characteristics suggest that the use of a flexible molecule provide an additional approach for fine-tuning magnetic interactions.

## Introduction

Molecule based magnetic materials are the focus of intense studies because they play key roles in the development of ferromagnets.[1,2] Many different molecular approaches have been engineered.[3,4] Among these, the nitroxide free radicals have been the subject of extensive investigations over many years, as they have a unique combination of chemical stability and versatility that makes them attractive candidates for spin labels and paramagnetic building blocks for the construction of multidimensional magnetic materials.[5] Landmark examples are the $\beta$-crystal phase of *p*-nitrophenyl nitronyl-nitroxide[6] and a diazaadamantane dinitroxide,[7] both

* To whom correspondence should be addressed. E-mail: ziessel@chimie.u-strasbg.fr.
[†] Laboratoire de Chimie Molculaire, Ecole de Chimie, Polymères et Matériaux (ECPM), UMR 7008, Université Louis Pasteur (ULP).
[‡] Université Joseph Fourier Grenoble 1.
[§] Institut Charles Sadron, Université Louis Pasteur (ULP).
[||] Institut Le Bel.



10.1021/ic020484v CCC: $25.00 
Published on Web 04/05/2003

of which undergo a transition into ferromagnetic states at cryogenic temperatures. Numerous interesting results have been obtained by coordinating directly nitronyl-nitroxide radicals to transition metal ions. However, most of the literature describes complexes engineered from strongly acidic metal centers often surrounded by hexafluoroacetylacetonate fragments.[8] The major drawback of such systems is the low dimensionality of the resulting materials owing to the bulkiness of the substituents and to the fact that only two vacant sites are available for ligation to the paramagnetic metal precursor. Nitroxides form complexes with metal halides, but when an additional donor atom is present on the platform, families of compounds with peculiar magnetic properties have been produced.[9] Since this discovery, it has been shown that chelating frameworks such as pyridine,[10] bipyridine,[11] phenanthroline,[12] or imidazole[13] could be grafted with nitronyl-nitroxides or imino-nitroxides in such a way to benefit from a chelating effect. This strategy gave new coordinating schemes and allowed coordination of weakly acidic and nonsterically encumbered metal ions. It is worth pointing out that, in some cases, the short linkage (a single C−C bond), between the chelate and the radical, forces the magnetic orbitals to adopt a nonideal orthogonal conformation which results in antiferromagnetic interactions.[11,12,14]

Furthermore, the syntheses of compounds containing flexible and pendent radical arms tethered to macrocyclic frames have been reported. These molecules were prepared by an O- or N-alkylation of cyclic phenols or secondary amines via a nucleophilic substitution of the chloride group from chloromethyl-nitronyl-nitroxide giving rise to spin-labeled calixarenes[15] and crown-ethers.[16] Recently, Rey and coworkers have reported flexible nitroxide ligand derivatives prepared from bromomethyl-nitronyl-nitroxide and *N*-methylethylenediamine or piperazine.[17] Their transition metal complexes were prepared independently from hexafluoroacetyl acetonate or perchlorate nickel salts,[18] illustrating the potential of this type of ligand in the design of new magnetic materials. Herein, we describe our attempts to achieve the synthesis of a novel ligand **1** which combines the ideas of having a good chelating platform and flexible spin-labeled pendent arms, a feature which has not been reported previously. The present work reveals that the ligand can adopt a meridional or a facial conformation, respectively, with Ni and Zn or with Cu. The magnetic and electronic properties are discussed in light of the molecular structures determined by X-ray diffraction on single crystals. The strength of these interactions has been correlated to suitable structural features.

## Experimental Section

**X-ray Crystal Structure Analysis.** The intensity data were collected in the $\varphi$ scan mode at 173 K on a KappaCCD diffractometer equipped with a graphite monochromator for the Mo K$\alpha$ radiation. Cell constants were derived from a least-squares fit of the setting angles for 25 selected reflections with $10° < \theta < 15°$. The intensities were corrected for Lorentz and polarization effects but not for absorption. The positions of the metal ions were found using the SHELX86 package.[19] The remaining atoms were located in a succession of difference Fourier syntheses and were refined with anisotropic thermal parameters using the SHELX76 package.[20] The hydrogen atoms were included in the final refinement model in calculated and fixed positions with isotropic thermal parameters. Crystal structure and refinement data are summarized in Table 1.

**Magnetic Susceptibility Measurements.** The magnetic susceptibility was measured on the bulk polycrystalline material in the 2−300 K temperature range for each compound with a Quantum Design MPMS superconducting SQUID magnetometer operating


(1) The literature on this topic is too large to be exhaustively quoted. For some recent, representative books and review articles, see: (a) Kahn, O. *Molecular Magnetism*; VCH: New York, 1993. (b) *Molecular Magnetism: From Molecular Assemblies to the Devices*; Coronado, E., Delhaes, P.; Gatteschi, D., Miller, J. S., Eds.; NATO ASI Series E 321; Kluwer Academic Publishers: Dordrecht, The Netherlands, 1996. (c) *Magnetism: Molecules to Materials. Models and Experiments*; Miller, J. S., Drillon, M., Eds.; Wiley-VCH: Weinheim, Germany, 2001. (d) VIIth International Conference on Molecular-based Magnets (ICMM 2000); San Antonio, TX, September 16−21, 2000, as described in *Polyhedron* **2001**, *20*, 1305.

(2) (a) Iwamura, H.; Koga, N. *Acc. Chem. Res.* **1993**, *26*, 346. (b) Rajca, A. *Chem. Rev.* **1994**, *94*, 871. (c) Hatlevik, *ϕ*.; Buschmann, W. E.; Zhang, J.; Manson, J. L.; Miller, J. S. *Adv. Mater.* **1999**, *11*, 914.

(3) (a) De Munno, G.; Julve, M.; Viau, G.; Lloret, F.; Faus, J.; Viterbo, D. *Angew. Chem., Int. Ed. Engl.* **1996**, *35*, 1807. (b) De Munno, G.; Poerio, T.; Viau, G.; Julve, M.; Lloret, F.; Yournaux, Y.; Rivière. *Chem. Commun.* **1996**, 2587. (c) Boskovic, C.; Pink, M.; Huffman, J. C.; Hendrickson, D. N.; Christou, G. *J. Am. Chem. Soc.* **2001**, *123*, 9914. (d) Miyazaki,Y.; Bhattacharjee, A.; Nakano, M.; Saito, K.; Aubin, S. M. J.; Eppley, H. J.; Christou, G.; Hendrickson, D. N.; Sorai, M. *Inorg Chem.* **2001**, *40*, 6632.

(4) (a) Larionova, J.; Gross, M.; Pilkington, M.; Andres, H.; Stoechli-Evans, H.; Guidel, H. U.; Decurtins, S. *Angew Chem., Int. Ed.* **2000**, *39*, 1605. (b) Barclay, T. M.; Hicks, R. G.; Lemaire, M. T.; Thompson, L. K. *Inorg. Chem.* **2001**, *40*, 6521.

(5) (a) Caneschi, A.; Gatteschi, D.; Sessoli, R.; Rey, P. *Acc. Chem. Res.* **1989**, *22*, 392. (b) Caneschi, A.; Gatteschi, D.; Rey, P. *Prog. Inorg. Chem.* **1991**, *39*, 331.

(6) Kinoshita, M.; Turek, P.; Tamura, M.; Nozawa, K.; Shiomi, D.; Nakazawa, Y.; Ishikawa, M.; Takahashi, M.; Awaga, K.; Inabe, T.; Maruyama, Y. *Chem. Lett.* **1991**, 1225.

(7) Chiarelli, R.; Novak, M. A.; Rassat, A.; Tholence, J.-L. *Nature* **1993**, *363*, 147.

(8) (a) Gatteschi, D.; Laugier, J.; Rey, P.; Zanchini, C. *Inorg. Chem.* **1987**, *26*, 938. (b) Caneschi, A.; Gatteschi, D.; Sessoli, R.; Hoffmann, S. K.; Laugier, J.; Rey, P. *Inorg. Chem.* **1988**, *27*, 2392. (c) Caneschi, A.; Ferraro, F.; Gatteschi, D.; Rey, P.; Sessoli, R. *Inorg. Chem.* **1990**, *29*, 4217.

(9) (a) Luneau, D.; Rey, P.; Laugier, J.; Fries, P.; Caneschi, A.; Gatteschi, D.; Sessoli, R. *J. Am. Chem. Soc.* **1991**, *113*, 1245. (b) Luneau, D.; Risoan, G.; Rey, P.; Grand, A.; Caneschi, A.; Gatteschi, D.; Laugier, J. *Inorg. Chem.* **1993**, *32*, 5616.

(10) Fegy, K.; Sanz, N.; Luneau, D.; Belorizky, E.; Rey, P. *Inorg. Chem.* **1998**, *37*, 4518.

(11) Luneau, D.; Laugier, J.; Rey, P.; Ulrich, G.; Ziessel, R.; Legoll, P.; Drillon, M. *J. Chem. Soc., Chem. Commun.* **1994**, 741.

(12) Ziessel, R. *Mol. Cryst. Liq. Cryst.* **1995**, *273*, 101.

(13) (a) Fegy, K.; Luneau, D.; Belorizky, E.; Novac, M.; Tholence, J.-L.; Paulsen, C.; Ohm, T.; Rey, P. *Inorg. Chem.* **1998**, *37*, 4524. (b) Fegy, K.; Luneau, D.; Ohm, T.; Paulsen, C.; Rey, P. *Angew. Chem., Int. Ed.* **1998**, *37*, 1270.

(14) Francese, G.; Romero, F. M.; Neels, A.; Stoeckli-Evans, H.; Decurtins, S. *Inorg. Chem.* **2000**, *39*, 2087.

(15) Ulrich, G.; Turek, P.; Ziessel, R. *Tetrahedron Lett.* **1996**, *37*, 8755.

(16) Ulrich, G.; Turek, P.; Ziessel, R.; De Cian, A.; Fischer, J. *J. Chem. Soc., Chem. Commun.* **1996**, 2461.

(17) Fegy, K.; Vostrikova, K. E.; Luneau, D.; Rey, P. *Mol. Cryst. Liq. Cryst.* **1997**, *305*, 69.

(18) Vostrikova, K. E.; Belorizky, E.; Pécaut, J.; Rey, P. *Eur. J. Inorg. Chem.* **1999**, 1181.

(19) Sheldrick, G. M. *Crystallographic Computing 3*; Sheldrick, G. M., Kruger, C., Goddard, R., Eds.; Oxford University Press: Oxford, U.K., 1985, p 175.

(20) Sheldrick, G. *System of Computing Programs*; University of Cambridge: Cambridge, England, 1976.

**Table 1.** Summary of the Crystal Structure Data Collection and Refinement for **1**, **2**, **3**, and **4**

| | **1** | **2** | **3** | **4** |
|---|---|---|---|---|
| formula | $C_{27}H_{37}N_7O_4$ | $C_{27}H_{39}N_7O_5Zn{\cdot}2ClO_4{\cdot}CH_2Cl_2$ | $C_{27}H_{39}N_7O_5Ni{\cdot}2ClO_4{\cdot}0.5CH_3OH{\cdot}0.5H_2O$ | $C_{27}H_{37}N_7O_4Cu{\cdot}2ClO_4{\cdot}CH_3CN$ |
| fw | 523.64 | 890.86 | 830.30 | 827.13 |
| $T$ (K) | 173 | 173 | 173 | 173 |
| cryst syst | triclinic | hexagonal | hexagonal | triclinic |
| space group | $P\bar{1}$ | $P3_2$ | $P3_2$ | $P\bar{1}$ |
| $Z$ | 2 | 3 | 3 | 2 |
| $a$ (Å) | 10.7224(4) | 15.4545(3) | 15.2867(1) | 11.8640(4) |
| $b$ (Å) | 11.0995(4) | 15.4545(3) | 15.2867(1) | 13.2032(4) |
| $c$ (Å) | 13.1134(3) | 13.5594(3) | 13.7160(1) | 13.2661(5) |
| α (deg) | 114.101(9) | 90 | 90 | 90.539(9) |
| $\beta$ (deg) | 97.476(9) | 90 | 90 | 104.983(9) |
| $\gamma$ (deg) | 99.667(9) | 120 | 120 | 113.252(9) |
| $V$ (Å$^3$) | 1369.7(4) | 2804.7(2) | 2775.78(6) | 1829.7(5) |
| $D_c$ (g·cm$^3$) | 1.27 | 1.58 | 1.49 | 1.50 |
| $\mu$(Mo Kα) (mm$^{-1}$) | 0.082 | 1.028 | 0.741 | 0.811 |
| GOF[a] | 1.213 | 1.330 | 1.416 | 1.556 |
| $R$ ($F_o$)[b] | 0.046 | 0.075 | 0.058 | 0.051 |
| $R_w$ ($F_o$)[c] | 0.061 | 0.096 | 0.075 | 0.078 |

[a] GOF = $[\sum w(|F_o|^2 - |F_c|^2)2/(n-p)]$. [b] $R(F_o) = \sum(|F_o| - |F_c|)/\sum|F_o|$. [c] $R_w(F_o) = \sum(w|F_o| - |F_c|)/\sum w|F_o|$.

at a field strength of 0.5 T or with a M 8100 SQUID susceptometer from Métronique operating at a field strength of 0.1 T. The data were corrected for magnetization of the sample holder contribution, and the magnetic susceptibilities were corrected for diamagnetism of the molecules by fitting the high temperature data of the $\chi{\cdot}T$ versus $T$ curve or by estimation of its contribution from suitable Pascal tables.

**EPR Measurements.** The EPR measurements were performed with an X-band (microwave frequency: ca. 9.8 GHz) spectrometer (Bruker ESP 300E) equipped with a rectangular TE 102 cavity. The available temperature range was 4−300 K with a continuous flow cryostat (Oxford ESR 900) operating with liquid helium. The temperature was accurately determined with a Au−Fe/Chromel thermocouple located within the sample tube close to the sample. The diluted solutions have been degassed upon bubbling Ar gas prior to all EPR studies, whether in fluid or in frozen state. Care has been taken in order to avoid microwave saturation phenomena or overmodulation effects on the EPR signal.

**Other Instrumentation.** UV−vis spectra were obtained on a Unikon 933 (Kontron Instruments) spectrophotometer. FT-IR spectra were obtained on a Bruker IFS 25 spectrometer using KBr pellets. Fast-atom bombardment (FAB, positive mode) was performed with a ZAB-HF-VG analytical apparatus in a *m*-nitrobenzyl alcohol (*m*-NBA) matrix.

**Materials.** 6-Aminomethyl-2,2′-bipyridine[21] and chloromethyl-nitronyl-nitroxide[22] were prepared using literature procedures. Perchlorate salts were used as purchased. *Perchlorate salts should be handled carefully, in low quantities, used as hydrated salts, and never dehydrated under vacuum before being used.*

**BpyN(NIT)$_2$, 1.** A suspension of 6-aminomethyl-2,2′-bipyridine (243 mg, 1.53 mmol), chloromethyl-nitronyl-nitroxyde (684 mg, 3.21 mmol), $K_2CO_3$ (446 nmg, 3.21 mmol), and KI (25.5 mg, 10 mol %) in acetonitrile (30 mL) was stirred at room temperature for 30 min. The violet mixture was then heated at 60 °C during 75 min. The resultant pink solution was quenched with water (20 mL) and extracted with $CH_2Cl_2$ (3 × 150 mL). The organic phase was dried over $MgSO_4$. Chromatography (silica flash, $CH_2C_2$ to $CH_2Cl_2$−6% MeOH) and subsequent recrystallization from a mixture of $CH_2C_2$/hexane gave pink crystals of **1** (519 mg, 65%). IR (KBr pellet, cm$^{-1}$) 1625, 1573, 1422, 1369, 1291, 1136, 1109. UV−vis ($CH_2Cl_2$) $\lambda$ (nm) ($\epsilon$ ($M^{-1}$ cm$^{-1}$)) 569 (sh, 2110), 536 (2520), 506 (sh, 1670), 327 (47460), 289 (27150), 245 (10500). FAB-MS (*m*-NBA) 524 [M − e]$^+$, 508 [M − O − e]$^+$, 492 [M − 20 − e] $^+$, 458 [M − 40 − 2H − e] $^+$. Anal. Calcd for $C_{27}H_{37}N_7O_4$ ($M_r$ = 523.64): C, 61.93; H, 7.12; N, 18.72. Found: C, 61.78; H, 7.03; N, 18.59.

**General Procedure for the Preparation of Complexes 2 and 3.** A violet solution of bpyN(NIT)$_2$ (60 mg scale) in dichloromethane (3 mL) was added to a solution of M(ClO$_4$)$_2$·6H$_2$O (1.1 equiv, M = Zn or Ni) in methanol (3 mL). After 5.5 h of stirring, the solution was filtered over Celite, and slow diffusion of $Et_2O$ gave crystals of the target complex.

**[Zn(bpyN(NIT)$_2$)](ClO$_4$)$_2$, 2.** Yield 85%. FT-IR (KBr pellets, cm$^{-1}$) 1609, 1458, 1424, 1377, 1303, 1176, 1112. UV−vis ($CH_3CN$) $\lambda$ (nm) ($\epsilon$ ($M^{-1}$ cm$^{-1}$)) 515 (1895), 325 (31300), 310 (45550), 301 (sh, 38300), 250 (10930). FAB-MS (*m*-NBA) 686.2 ([M − ClO$_4$]$^+$,100), 587.2 ([M − 2ClO$_4$ − e]$^+$, 20), 571.2 ([M − 2Cl$_4$ − O − e]$^+$, 15), 539.1 ([M − 2Cl$_4$ − 3O − e]$^+$, 5). Anal. Calcd for $C_{27}H_{37}N_7O_{12}C_{12}Zn$ (M = 787.92): C, 41.16; H, 4.73; N, 12.44. Found: C, 41.08; H, 4.52; N, 12.27.

**[Ni(bpyN(NIT)$_2$)](ClO$_4$)$_2$, 3.** Yield 89%. IR (KBr pellet, cm$^{-1}$) 1614, 1457, 1379, 1300, 1178, 1112. UV−vis ($CH_3CN$) $\lambda$ (nm) ($\epsilon$ ($M^{-1}$ cm$^{-1}$)) 543 (sh, 2250), 518 (2635), 332 (sh, 17360), 307 (34220), 299 (sh, 30690), 244 (13840). FAB-MS (*m*-NBA) 680.5 ([M − ClO$_4$]$^+$, 100), 664.5 ([M − ClO$_4$ − O]$^+$, 20), 648.5 ([M − ClO$_4$ − 2O]$^+$, 20), 581.4 ([M − 2ClO$_4$ − e]$^+$, 50), 549.2 ([M − 2ClO$_4$ − 2O − e]$^+$, 5). Anal. Calcd for $C_{27}H_{37}N_7O_{12}C_{12}Ni$ ($M_r$ = 781.24): C, 41.51; H, 4.77; N, 12.55. Found: C, 41.57; H, 4.82; N, 12.67.

**[Cu(bpyN(NIT)$_2$)(C1O$_4$)$_2$, 4.** Addition of a violet solution of bpyN(NIT)$_2$ (51.7 mg, 0.099 mmol) in $CH_2Cl_2$ p.a. (3 mL) to a solution of Cu(ClO$_4$)$_2$·6H$_2$O (37.4 mg, 1.1 equiv) in MeOH p.a. (3 mL) led immediately to the formation of a red precipitate. The dark solution was still stirred for 4.5 h. The solid was centrifuged and washed with $Et_2O$. Recrystallization from a mixture of MeCN/$Et_2O$/hexane gave the violet complex **4** (60 mg, 73%). FT-IR (KBr pellets, cm$^{-1}$) 1612, 1458, 1424, 1377, 1308, 1108. UV−vis ($CH_3CN$) $\lambda$ (nm) ($\epsilon$ ($M^{-1}$ cm$^{-1}$)) 503 (1950), 429 (2040), 313 (34070), 303 (sh, 31000), 255 (13110). FAB-MS (*m*-NBA): *m*/*z* 685.6 ([M − ClO$_4$]$^+$, 100), 669.6 ([M − ClO$_4$ − O]$^+$, 30), 653.6 ([M − ClO$_4$ − 2O]$^+$, 10), 586.5 ([M − 2ClO$_4$ − e]$^+$, 70), 570.4 ([M − 2ClO$_4$ − O − e]$^+$, 10), 538.4 ([M − 2ClO$_4$ − 30 − H − e]$^+$, 5). Anal. Calcd for $C_{27}H_{37}N_7O_{12}C_{12}Cu + CH_3CN$ ($M_r$ = 786.09 + 41.05): C, 42.11; H, 4.87; N, 13.55. Found: C, 41.97; H, 4.59; N, 13.25.

(21) Ziessel, R.; Lehn, J.-M. *Helv. Chim. Acta* **1990**, *73*, 1149.
(22) Ulrich, G. Thèse de l'Université Louis Pasteur, Strasbourg, France, 1996.

**Scheme 1**

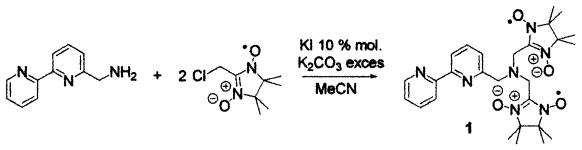


**Computational Details.** Calculations with the extended Hückel theory[23] (EHT) using the fragment molecular orbital approach[24] have been performed using the program ICON8.0. Extended Hückel parameters for Ni and Cu are taken from ref 25. Calculations at the CASSCF level have been performed using the MOLCAS5 package[26] and the energy-consistent small-core RECPs and their corresponding optimized basis sets of Stuttgart.[27] The molecule has been oriented such that the metal atom is at the center, the bipyridine lies in the *xy* plane, and the oxygen of the equatorial nitroxide on the O *x* axis. In the ab initio calculations, the perchlorate of the coordination sphere has been replaced by a hydroxide, and the 8 methyl groups have been replaced by hydrogen atoms. The plots of the molecular orbitals represent 3D isodensity surfaces (value = 0.03) drawn with MOLDEN.[28]

## Results and Discussion

**Synthesis.** This protocol was inspired by previous substitution of macrocyclic platforms with methyl-nitronyl-nitroxide templates.[15,16] Ligand **1** was prepared by nucleophilic substitution of chloromethyl-nitronyl-nitroxide by 6-aminomethyl-2,2′-bipyridine as sketched in Scheme 1. This reaction takes place under mild basic conditions in the presence of KI which ensured an in-situ exchange of chloride for the more labile iodine group. The stable ligand shows the characteristic pink color of an aminomethyl-nitronyl-nitroxide.[29] The N−O stretching vibration is characteristic of an NIT radical, and the FAB mass spectrum exhibits an intense molecular peak with fragmentation peaks due to the successive loss of the oxygen atoms, in agreement with the expected formula.

Mixing a slight excess of ligand **1** with the corresponding metal salt is accompanied by a pronounced color change from light pink to intense red. The FAB mass spectra of the resulting complexes show an intense molecular peak with the expected isotopomer distribution and the loss of a perchlorate anion with several fragments corresponding to the successive loss of oxygen atoms and/or the second perchlorate anion. The absence of any significant peaks at higher mass and peaks resulting from the presence of multicharged species excludes the presence of polynuclear species. The N−O stretching frequencies are shifted to higher values, pointing to the coordination of both NIT radicals to the metal center. In order to precisely determine the nature of the first coordination sphere of each metal and to understand how the ligand wraps around the metal center, the crystal structures of the ligand and of all complexes have been determined.

**Scheme 2**

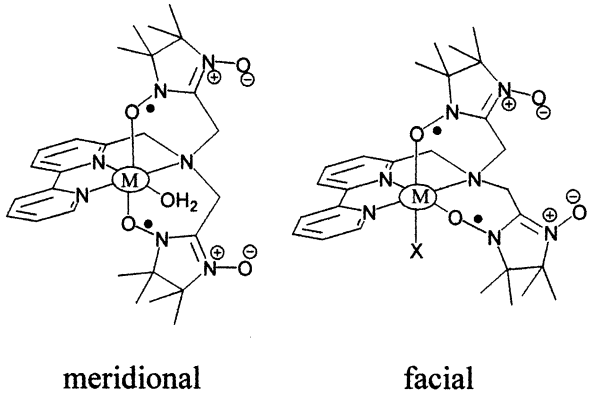


**Structural Details.** For each complex, ligand **1** behaves as a pentadentate chelate with two N(bpy), one N(amino) (labeled N(3) in the figures of the complexes), and two O(nitroxyl) atoms coordinated to the metal. The first coordination sphere is completed by one water molecule (for **2** and **3)** or one perchlorate anion (for **4)** providing in each case an axially distorted octahedron. Compounds **2** and **3** have identical geometrical features with the ON(3)O set of donor atoms in a meridional conformation (Scheme 2). These heteroatoms belong to the two oxygen atoms of the nitroxides (O) and to the nitrogen atom of the tertiary amine (N(3)). For compound **4**, one radical lies in an apical position and the second radical in the basal plane providing a facial conformation. Selected crystallographic data are gathered in Table 1.

**BpyN(NIT)$_2$, 1.** The crystal structure of the free ligand shows a transoid arrangement of the two pyridine rings in order to reduce the electronic repulsion of the N lone pairs as previously reported for related bpy compounds.[30] The N(amino) atom lies also trans versus the central pyridyl ring, forming a dihedral angle of 12.4°, while the dihedral angle between the two pyridine rings is 6.9°. This nearly planar conformation is similar to a terpyridine type of structure (Figure la).[31]

Both nitronyl-nitroxyde radicals feature bond lengths and angles similar to those found in uncoordinated NIT radicals (Table 2). Interestingly, one of the radicals is nearly

(23) (a) Hoffmann, R. *J. Chem. Phys.* **1963**, *39*, 1397. (b) Hoffmann, R.; Lipscomb, W. N. *J. Chem. Phys.* **1962**, *36*, 3179; **1962**, *37*, 2872.
(24) (a) Hoffmnann, R. *Science* **1981**, *211*, *995*. (b) See also: Albright, T. A.; Burdett, J. K.; Whangbo, M. H. *Orbital Interactions in Chemistry*; J. Wiley and Sons: New York, 1985.
(25) Tatsumi, K.; Nakamuna, A.; Hofmann, P.; Stauffert, P.; Hoffmann, R. *J. Am. Chem.* Soc. **1985**, *107*, 444.
(26) Andersson, K.; Barysz, M.; Bernhardsson, A.; Blomberg, M. R. A.; Carissan, Y.; Cooper, D. L.; Cossi, M.; Fleig, T.; Filscher, M. P.; Gagliardi, L.; de Graaf, C.; Hess, B. A.; Karlström, G.; Lindh, R.; Malmqvist, P.-Å; Neogrády, P.; Olsen, J.; Roos, B. O.; Schimmelpfennig, B.; Schtitz, M.; Seijo, L.; Serrano-Andrds, L.; Siegbahn, P. E. M.; Stålring, J.; Thorsteinsson, T.; Veryazov, V.; Wierzbowska, M.; Widmark, P.-O. *MOLCAS*, version 5.2; Lund University: Sweden, 2001.
(27) (a) Bergner, A.; Dolg, M.; Kuechle, W.; Stoll, H.; Preuss, H. *Mol. Phys.* **1993**, *80*, 1431. (b) Dolg, M.; Wedig, U.; Stoll, H.; Preuss, H. J. *Chem. Phys.* **1987**, *86*, 866.
(28) Schaftenaar, G.; Noordik, J. H. J. *Comput.-Aided Mol. Des.* **2000**, *14*, 123.
(29) Ullman, E. F.; Osiecki, J. H.; Boocock, D. G. B.; Darcy, R. *J. Am. Chem. Soc.* **1972**, *94*, 7049.
(30) (a) Merritt, L. L., Jr.; Schroeder, E. D. *Acta Crystallogr.* **1956**, *9*, 801. (b) Nakatsu, K.; Yoshioka, H.; Matsui, M.; Koda S.; Ooi, S. *Acta Crystallogr., Sect. A* **1972**, 24. (c) Chisholm, M. H.; Huffman, J. C.; Rothwell, I. P.; Bradley, P. G.; Kress N.; Woodruff, W. H. *J. Am. Chem. Soc.* **1981**, *103*, 4945.
(31) Harriman, A.; Hissler, M.; Ziessel, R.; De Cian, A.; Fischer, J. *J. Chem. Soc., Dalton Trans.* **1985**, 4067.

**Table 2.** Selected Bond Lengths (Å) of the Radical bpyN(NIT)$_2$, **1**

| | | | |
|---|---|---|---|
| C2−N2 | 1.33 | C10−N4 | 1.34 |
| C2−N3 | 1.34 | C10−N5 | 1.34 |
| N2−O1 | 1.28 | N4−O3 | 1.28 |
| N3−O2 | 1.28 | N5−O4 | 1.29 |

perpendicular to the other, pointing its oxygen atom toward the center of the second five-membered ring, a feature auspicious for ferromagnetic behavior. The distance between O3 and the nearby ONCNO plane is 3.73 Å while the nearest atom of the five-membered ring is N2 ($d_{O3\cdots N2}$ = 3.77Å). The angles necessary to give the relative position of the radicals are N4−O3−N2 = 117.1°, O3−N2−C2 = 80.6°, C10−N4−O3−N2 = 0°, N4−O3−N2−C2 = 64.2°, O3−N2−C2−Cl = −90.2°. Close examination of the crystal packing shows that the molecules are arranged in a head-to-tail fashion with relatively long intermolecular distances (Figure lb). On one side, two N−O groups of neighboring molecules are arranged in a head-to-tail fashion with the following geometrical data: O4···N5″ = 4.73 Å, O4−N5″−O4″ = 95°, C10−N5−O4−N5″ = 87.5°. On the other side of the molecule, the two radicals are more superimposed than in the precedent case with the shortest distance found between O1···N3′ (4.87 Å), C2−N3−O1′ 95.4°, N3−O1′−N2′ = 87.5°, C2−N3−O1′−N2′ = 15.8°, Cl−C2−N3−O1′ = 95.8°, N3−Ol′−N2′−C2′ = 98.5°.

**[Zn(bpyN(NIT)$_2$)·H$_2$O](ClO$_4$)$_2$·CH$_2$Cl$_2$, 2.** Here, the unit cell contains [Zn(bpyN(NIT)$_2$)·H$_2$O]$^{2+}$, two uncoordinated perchlorates, and a $CH_2Cl_2$ molecule. An ORTEP view of the cation is given in Figure 2. The zinc atom is surrounded by the three N atoms of the amino-bipyridine fragment and three O atoms belonging to the water molecule and the two nitroxide radicals, providing an axially distorted octahedral complex. The apical positions are occupied by the two nitrogens atoms N1 and N3 (highest metal−ligand distances, Table 3), while the basal plane is formed by the three oxygen atoms and the N2 nitrogen atom of the bipyridine fragment. The ON(3)O set of atoms lies in a meridional conformation. As expected, the NO bond lengths of the coordinated oxygen atoms are significantly longer than the free NO bonds (Table 4).

The dihedral angles between the two pyridine rings and the amino-pyridine fragment are, respectively, 3.6° and 9.4°. The Zn−O3−N5 and Zn−O5−N7 angles are 121.9° and 119.70°, and the dihedral angles Zn−O3−N5−C13 and Zn−O5−N7−C21 are, respectively, 30.2° and 38.1°. The intermolecular contacts between neighboring N−O groups are greater than 4 Å.

Despite the long distance (O2−C13′ = 4.22 Å), the intermolecular packing shows one radical pointing its oxygen atom toward the central carbon of the second radical with the following geometrical parameters: N4−O2−C13′ = 120.3°, O2−C13′−C12′ = 35.8°, N4−O2−C13′−C12′ = 152.3°, C13−N4−O2−C13′ = 159.8°, O2−C13′−N4′−O2′ = 39.4°.

**[Ni(bpyN(NIT)$_2$)·H$_2$O](ClO$_4$)$_2$·0·5CH$_3$OH·0.5H$_2$O, 3.** The unit cell contains one [Ni(bpyN(NIT)$_2$)·H$_2$O]$^{2+}$, two uncoordinated perchlorates, one-half molecule of methanol, and one-half molecule of water. The nickel(II) is coordinated

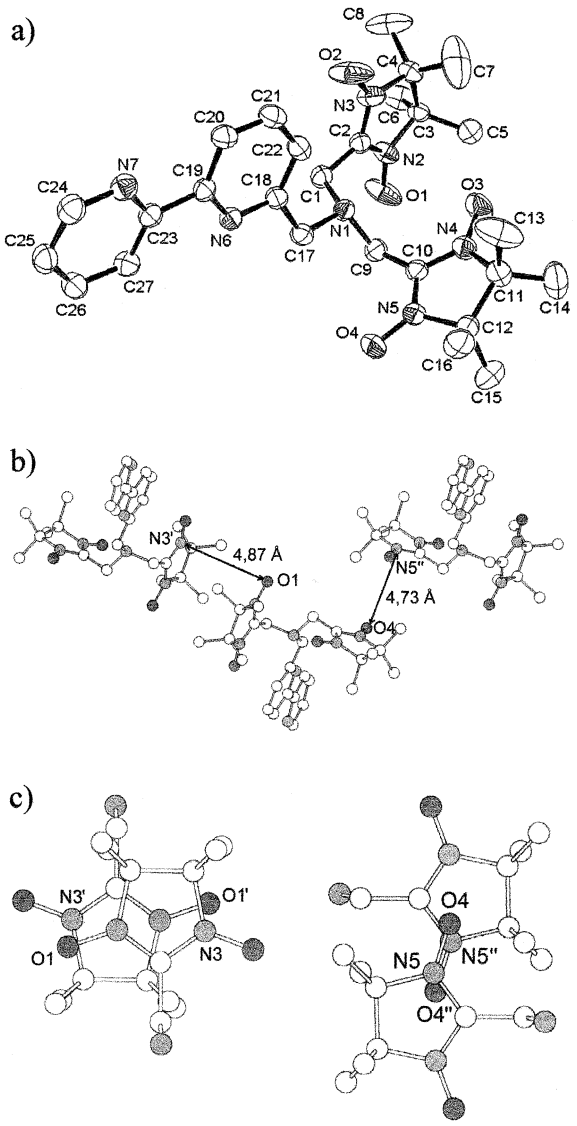


**Figure 1.** (a) ORTEP of ligand **1** drawn at the 30% probability level. Hydrogen atoms have been omitted for the sake of clarity. (b) Head-to-tail intermolecular dispositions of the radicals along a crystallographic chain. (c) O1···N3′ intermolecular contact.

by one pentadentate ligand and one water molecule giving rise to an axially distorted octahedral geometry. An ORTEP view of the cation is given in Figure 3. The Ni(II) complex has geometrical features similar to those of the zinc complex **2**. The three oxygen atoms of the radicals, the water molecule, and the N2 atom of the bipyridine subunit form the basal plane, while the ON(3)O set of atoms provides a meridional configuration around the nickel center. The apical positions are occupied by two nitrogen atoms N1 and N3 belonging, respectively, to the bipyridine and tertiary amine fragments, as previously described for the zinc complex.

The tilt angle between the two pyridine rings is 3.3°, whereas the angle between the amino group and the central pyridine is 4.2°. It is worth noting that the Ni···N(3) bond length is slightly longer (2.161 Å) than the Ni···$N_{bpy}$ bonds while the pyridine adjacent to the aliphatic N atom forms a shorter bond due to the shape of the ligand (1.964 versus 2.071 Å for the external pyridine−nickel bond distance). Other relevant geometrical features of the nickel complex

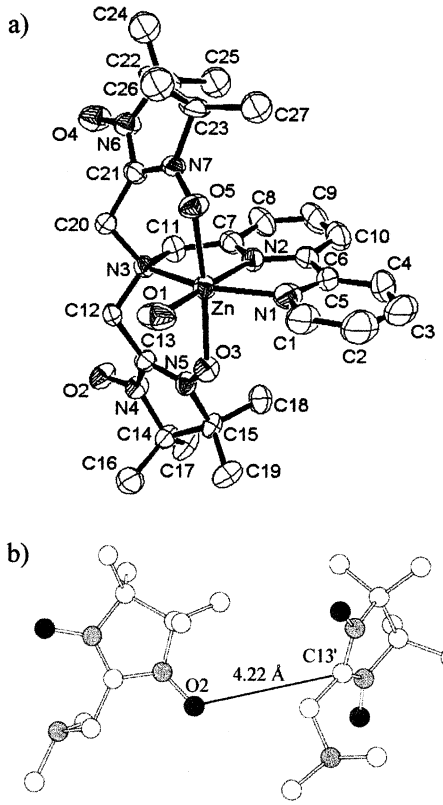


**Figure 2.** (a) ORTEP of complex **2** drawn at the 30% probability level. Hydrogen atoms have been omitted for the sake of clarity. (b) Intermolecular contact between O2 and C13′.

**Table 3.** Selected Bond Lengths around the First Coordination Sphere of the Metal (Å)[a]

| | **2**, M = Zn | **3**, M = Ni | **4**, M = Cu |
|---|---|---|---|
| $MN_1$ | 2.15(1) | 2.071(7) | 1.983(3) |
| $MN_2$ | 2.077(9) | 1.964(7) | 1.895(3) |
| $MN_3$ | 2.286(8) | 2.161(7) | 2.070(3) |
| MO | 2.078(7) | 2.050(6) | 1.914(2)[b] |
| MO′ | 2.110(7) | 2.030(6) | 2.429(3) |
| MO″[c] | 2.039(9) | 2.052(7) | 2.473(3) |

[a] O and O′ are the coordinated oxygen atoms of the radicals. [b] Radical in the equatorial position. [c] O″ is the oxygen atom of a water molecule (for M = Zn or Ni) or a perchlorate anion (for M = Cu).

**Table 4.** Selected Bond Lengths (Å)

| | **2** | **3** | **4** |
|---|---|---|---|
| $C_{13}N_4$ | 1.36(1) | 1.36(1) | 1.349(4) |
| $C_{13}N_5$ | 1.31(1) | 1.29(1) | 1.320(4) |
| $N_{40}O_{nc}$ | 1.27(1) | 1.28(1) | 1.281(4) |
| $N_5O_c$ | 1.32(1) | 1.306(9) | 1.298(3)[a] |
| $C_{21}N_6$ | 1.36(1) | 1.35(1) | 1.358(5) |
| $C_{21}N_7$ | 1.31(1) | 1.32(1) | 1.309(4) |
| $N_6O_{nc}$[b] | 1.28(1) | 1.273(9) | 1.260(4) |
| $N_7O_c$[c] | 1.33(1) | 1.317(8) | 1.311(4)[d] |

[a] Radical in the axial position. [b] nc accounts for noncoordinated. [c] c accounts for coordinated. [d] Radical in the equatorial position.

are the following: (i) the Ni−O3−N5 and Ni−O5−N7 angles are 119.7° and 121.5°, and the dihedral angles Ni−O3−N5−C13 and Ni−O5−N7−C21 are, respectively, 36.5° and 28.4°; (ii) both radicals slightly deviate from the axial axis toward the amino-pyridyl moiety by ca. 5°. Intermolecular contacts between neighboring N−O groups are greater than 4 Å.

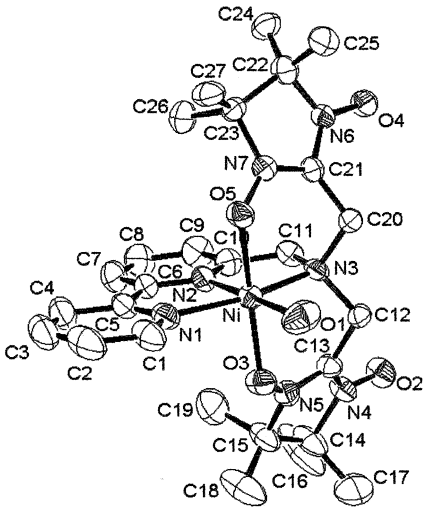


**Figure 3.** ORTEP of complex **3** drawn at the 30% probability level. Hydrogen atoms have been omitted for the sake of clarity.

**$[Cu(bpyN(NIT)_2)](ClO_4)_2 \cdot CH_3CN$, 4.** The unit cell consists of one $[Cu(bpyN(NIT)_2)]^{2+}$, one coordinated perchlorate, one uncoordinated perchlorate, and an acetonitrile molecule. As shown in the ORTEP view (Figure 4a), the copper(II) is surrounded by one $bpyN(NIT)_2$ ligand and the O atom of a perchlorate. Interestingly, one radical is coordinated within the basal plane whereas the second radical lies in an apical position. Contrary to the previous molecular structures, the ON(3)O set of atoms provides a facial conformation.

The basal plane is provided by the three N atoms of the amino-bipyridine ligand and a nitroxide O atom of one NIT radical. Within this plane, the N−Cu bond lengths are in the same range as described for the previous structures, with a very short Cu−O4 distance of 1.91 Å. In the apical position, the distance between the O atom of the second radical and the copper ion is much longer (2.43 Å). The perchlorate O atom is loosely bonded with a distance of 2.47 Å from the metal center in the second apical position (Table 3). The dihedral angles between the two pyridine rings and between the amino-pyridine fragment and the adjacent pyridine are 0.9° and 13.6°, respectively. The Cu−O2−N5 and Cu−O4−N7 angles are 110.3° and 119.0°, and the dihedral angles Cu−O2−N5−C13 and Cu−O4−N7−C21 are, respectively, 38.0° and 15.2°. Furthermore, the mean plane of the radical in the apical position[11] versus the plane containing the $d_{x^2-y^2}$ magnetic orbital of the copper(II) is 51.0° whereas the analogous angle with the radical in the basal position is only 26.4°. Intermolecular contacts which may account for the magnetic exchange pathways have been analyzed. The shortest NO distances of neighboring molecules are 3.70 Å for O1···O3′ and 3.88 Å for O1···O1′ forming a dimer (Figure 4b). It should be noticed that the angle C13−N4−O1−O′1 is 4.7° which shows that both radicals lie in the same plane. These dimers are connected in a head-to-tail arrangement, at a distance of 4.39 Å, to form crystallographic chains running along the $(x + 1, y + l, z)$ direction. Under these conditions, the overlapping between the $\pi^*$ orbitals of the radicals is efficient despite the fact that the distances are relatively long.

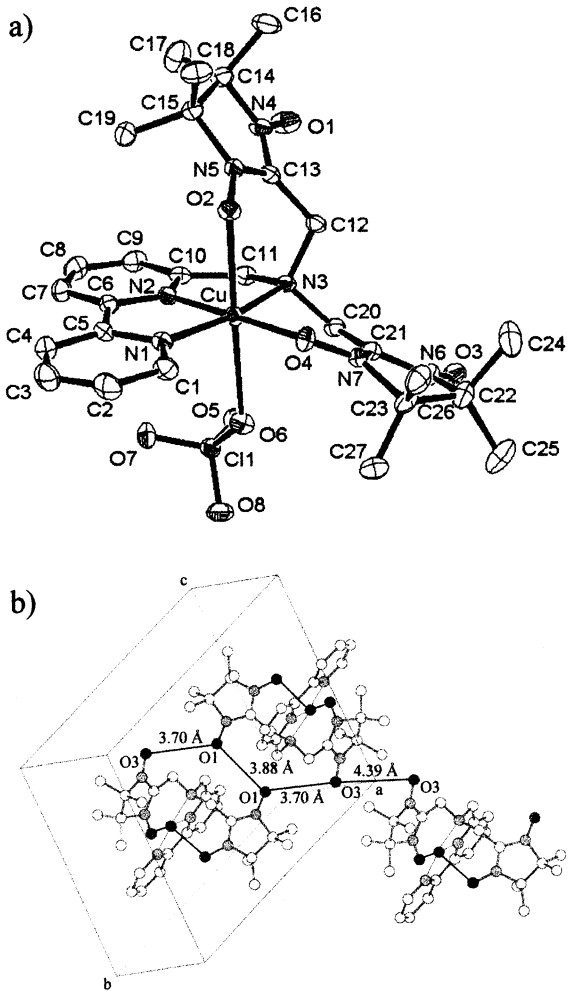


**Figure 4.** (a) ORTEP of complex **4** drawn at the 30% probability level. Hydrogen atoms have been omitted for the sake of clarity. (b) Intermolecular contacts between molecules of **4** running along the ($x + 1$, $y + 1$, $z$) direction.

**Magnetic and EPR Properties.** The magnetic susceptibility $\chi$ versus absolute temperature has been measured from room temperature to 2 K for the four compounds on microcrystalline samples.

**BpyN(NIT)$_2$, 1.** The value of $\chi \cdot T = 0.74$ emu·K·mol$^{-1}$ at room temperature (rt) is close to the expected value for two uncorrelated spins $S = {}^1/_2$ ($\chi T = 0.75$ emu·K·mol$^{-1}$). On lowering the temperature, $\chi \cdot T$ remains nearly constant until ca. 50 K, and then, it increases to a maximum of 0.78 emu·K·mol$^{-1}$ at 26 K (Figure 5a). A sharp decrease down to 0.53 emu·K·mol$^{-1}$ is observed at 2 K. Different options could be used to fit the magnetic behavior: (i) A $1/\chi$ versus $T$ curve of the high temperature regime above 25 K could be modeled with a Curie−Weiss law giving a positive Weiss temperature $\theta = 1.7$ K (Figure 5b). (ii) In light of the X-ray structure, one meaningful model which can be used to fit the data is an alternating 1D chain with two different intermolecular interactions. As a matter of fact this model does not fit the experimental curve. (iii) However, a good fit was obtained by using a dimeric two spin $S = {}^1/_2$ system

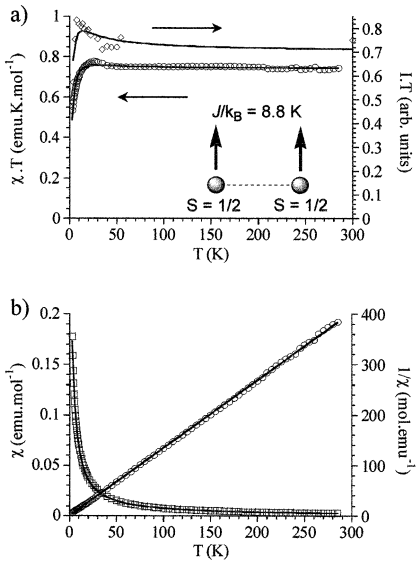


**Figure 5.** (a) Static $\chi \cdot T$ versus $T$ curve of compound **1** (○). EPR normalized $I \cdot T$ versus $T$ curve (◇). The solid lines represent the best fits. (b) Static $\chi$ versus $T$ (□) and $1/\chi$ versus $T$ (○) curves of compound 1.

($H = -2J\mathbf{S}_1 \cdot \mathbf{S}_2$)[33] with a mean field correction ($\theta$) which averages the intermolecular interactions. An exchange interaction of $J/k_B = 8.8 \pm 0.5$ K with $\theta = -3.1 + 0.1$ K provides a good agreement with the experimental data (Figure 5a). In order to exclude the presence of an artifact during the susceptibility measurements and to prove that the increase of the magnetic moment in the solid state stems from a genuine intramolecular ferromagnetic interaction between both radicals, we have undertaken EPR measurements in solution but also in the solid state.

The EPR signal of a polycrystalline powder (the same sample which has been used for the previous magnetic measurements) has been recorded between 4 and 55 K. The single Lorentzian line of the $\Delta M_s \pm 1$ transition has a peak-to-peak line width varying between ca. 13 G at 4 K and 7.5 G at 50 K. The shape of this line does not vary significantly. Although a half-field resonance line ($\Delta M_S = \pm 2$) is observed within this temperature range, it is too weak to estimate its temperature dependence. The temperature dependence of the main resonance line is plotted as the $I \cdot T = f(T)$ curve in Figure 5a, where $I$ represents the usual EPR intensity obtained by double integration of the first derivative of the absorption signal. As the temperature decreases below 50 K, $I \cdot T$ is increasing up to a maximum at 10 K, followed by a sharp decrease at lower temperature. A very weak variation of the $g$ factor below 10 K is observed which would suggest the absence of any phase transition ($g = 2.0072$ at 4 K and 2.0068 above 8 K). This behavior is in excellent agreement with the SQUID measurements. The slight difference in the sharpness of both experimental results is due to the slow variation and the more precise EPR technique, which discards the diamagnetic part of the sample and the sample holder. These data could be satisfactorily fitted using a Bleaney−Bowers expression ($H = -2J\mathbf{S}_1 \cdot \mathbf{S}_2$) providing an intramo-

(32) Borris-Almenar, J. J.; Coronado, E.; Curely, J.; Georges, R.; Gianduzzo, J. C. *Inorg. Chem.* **1994**, *33*, 5171.

(33) Bleaney, B.; Bowers, K. D. *Proc. R. Soc. (London), Ser. A* **1952**, *214*, 451.

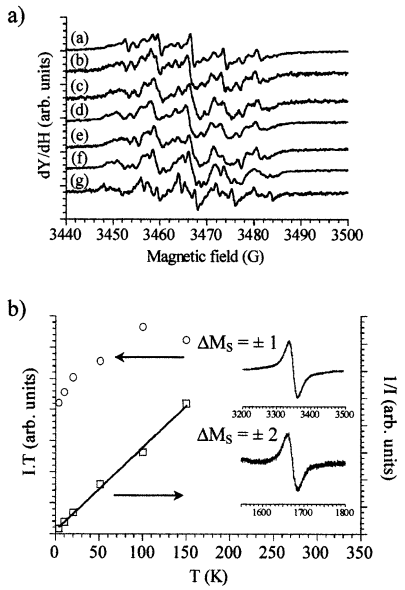


**Figure 6.** (a) Diluted solution spectra of compound **1** in (a) hexane, (b) THF, (c) acetone, (d) dichloromethane, (e) acetonitrile, (f) methanol, and (g) methanol/water 1/1. (b) Frozen dichloromethane solution EPR spectra of compound **1**. $I{\cdot}T$ versus $T$ (○) and $1/I$ versus $T$ (□) curves. Inserts: shape of the $\Delta M_s = \pm 1$ and $\Delta M_s = \pm 2$ lines.

lecular ferromagnetic interaction of $J/k_B = 11 \pm 6$ K with a mean field interaction $\theta$ of $-1.6 \pm 0.4$ K.

In order to check if this ferromagnetic interaction persists in solution, various solvents (hexane, THF, acetone, dichloromethane, acetonitrile, methanol, and a 1/1 mixture of methanol and water) have been used to prepare diluted fluid solutions (Figure 6a). The observed EPR spectra at room temperature show multiple components due to an overlapping of different signals belonging to weakly and strongly coupled diradicals in various conformations. This is a clear evidence of the flexibility of the two pendent radical arms in fluid solution, a situation previously found in bis-TEMPO radicals bridged by poly(ethylene glycol) chains.[34] In dichloromethane, the EPR spectra were recorded between 4 and 150 K. As shown in the insets of Figure 6b, a main resonance line is observed at $g = 2.0069$, and a half-field signal is observed at $g \approx 4.02$. As a consequence of the flexibility of the radical in fluid solution, the maximum in the $\chi{\cdot}T$ curve observed in the crystalline state is not observed under these experimental conditions. The reciprocal EPR susceptibility is continuously decreasing with lowering the temperature and could be fitted with a Curie−Weiss law with $\theta = -4.4 \pm 0.7$ K (see Figure 6b).

Interestingly, when the ligand is studied in a matrix of dichloromethane/methanol 1/1 versus the temperature, new well defined lines appear as shown in Figure 7a. In the temperature range 4−20 K, the spectra remain unchanged, with a central line at $g = 2.006$ due to the doublet state and lines corresponding to a triplet state. At low temperature, a signal centered at $g \approx 4.02$ with a line width of 15.6 G is also observed. The doublet state probably results from a situation where both radicals are not or weakly coupled.

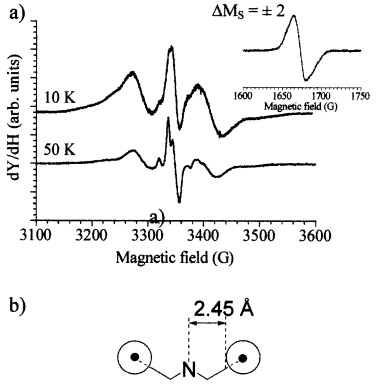


**Figure 7.** (a) Frozen dichloromethane/methanol 1/1 solution EPR spectra of compound **1** at 10 and 50 K. Insert: shape of the $\Delta M_s = \pm 2$ line. (b) Schematic representation of the distance between the radicals of ligand **1** in its most extended form.

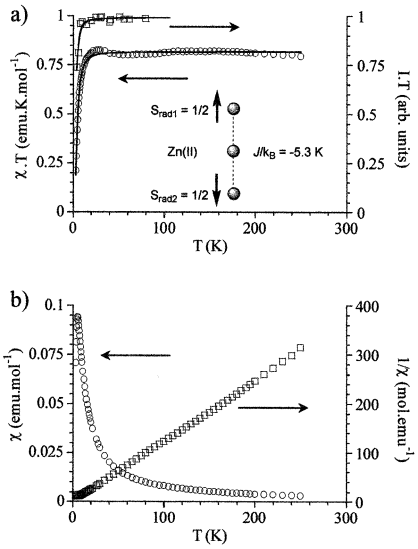


**Figure 8.** (a) Static $\chi{\cdot}T$ versus $T$ curve of compound **2** (○). EPR normalized $I{\cdot}T$ versus $T$ curve (□). The solid lines represent the best fits. (b) Static $\chi$ versus $T$ (□) and $1/\chi$ versus $T$ (○) curves of compound **2**.

Furthermore, using the point dipole approximation, it was possible to estimate a distance of ca. 5.8 Å between both radicals ($D' = 27810/d^3$, where $D'$ accounts for the half distance measured in gauss between the most external lines of the triplet pattern and $d$ is the average distance between the two radicals in angstroms (Figure 7b)).[35] This distance is larger than in the solid state ($d = 4.90$ Å), clearly showing that under these conditions the two radicals in **1** are in a more extended conformation, a situation where ferromagnetic coupling is not favorable.

**$[Zn(bpyN(NIT)_2){\cdot}H_2O](ClO_4)_2$, 2.** The shape of the $\chi{\cdot}T$ versus $T$ curve is similar to that of the free ligand **1**. The high temperature value is close to 0.8 emu·K·mol$^{-1}$ and is in keeping with the theoretical value calculated for two uncorrelated spins ($\chi{\cdot}T = 0.75$ emu·K·mol). Upon decreasing the temperature, the overall deviation from this value is less than 2% above 25 K (Figure 8a). A maximum is observed at 5 K in the susceptibility $\chi$ versus $T$ (Figure 8b). A good fitting of the experimental data is obtained by taking into account a dimeric model of two

(34) Gagnaire, G.; Jeunet, A.; Pierre, J.-L. *Tetrahedron Lett.* **1989**, *30*, 101.

(35) Rassat, A. *Pure Appl. Chem.* **1971**, *25*, 623.

$^1/_2$ spins ($H = -2J\mathbf{S}_1\cdot\mathbf{S}_2$) with a mean field correction. An antiferromagnetic intramolecular interaction of $J/k_B = -5.3 \pm 0.3$ K and a positive intermolecular interaction $\theta = 2.0 \pm 0.4$ K is obtained for the $\chi\cdot T$ curve. This exchange interaction is reasonably explained by means of a superexchange mechanism through the diamagnetic zinc ion. Several examples of this kind of magnetic coupling have previously been described, e.g., in metal semiquinonato[36] and spin-labeled terpyridine[37] complexes where appropriate metal and radical energetic states are close in energy and blended throughout the metallic core. A ferromagnetic interaction is also found, according to the positive Weiss temperature obtained by fitting the $1/\chi$ versus $T$ curve ($\theta = 0.6 \pm 0.5$ K above 25 K). Close examination of the crystal packing reveals a quasi orthogonality of the two radicals in the solid state, and despite the large radical−radical distances ($d >$ 4.0 Å), a through space interaction could not be completely ruled out.

The EPR spectra of an acetonitrile frozen solution shows a half field signal at $g \approx 4$ together with the main resonance at $g = 2.007$ at 4, 20, and 50 K. In a frozen acetonitrile matrix, the shape and the width of the main signal, consisting of a single line, is constant over the whole range of temperature. The $I\cdot T$ versus $T$ curve, represented in Figure 8a, shows a sharp decrease below 10 K. Above this temperature, the curve is linear, confirming that only a weak antiferromagnetic interaction is operating at very low temperature. The overall behavior could be parametrized with a Bleaney−Bowers expression ($H = -2J\mathbf{S}_1\cdot\mathbf{S}_2$) with a negative value of $J/k_B = -1.7 \pm 0.2$ K. The very weak intermolecular ferromagnetic interaction previously found in the bulk material is not found in diluted and frozen solutions.

**[Ni(bpyN(NIT)$_2$)·H$_2$O](ClO$_4$)$_2$, 3.** At room temperature, the product of $\chi\cdot T$ (1.12 emu·K·mol$^{-1}$) is lower than the expected value for two uncorrelated radicals ($S = ^1/_2$) and a high spin Ni(II) ($S = 1$) with $g = 2.2$ (theoretical calculated value $\chi\cdot T$= 1.96 emu·K·mol). By lowering the temperature, the curve decreases rapidly down to nearly 0 at ca. 50 K (Figure 9a). It is worth mentioning that the susceptibility $\chi$ exhibits a minimum at 30 K. The magnetic susceptibility measurements have been realized two times, using two different techniques with the same sample recrystallized a second time under similar conditions. Increasing the temperature to 400 K does not allow the susceptibility to reach the plateau usually expected at high temperature, when all the spins are independent. According to the structural data, complex **3** is best described as isolated molecular units. Therefore, the magnetic behavior is described on the basis of an asymmetric linear radical−Ni(II)−radical trimer model corresponding to the following spin Hamiltonian (eq 1):

$$H_{ex} = -2J\mathbf{S}_1\cdot\mathbf{S}_2 - 2J'\mathbf{S}_1\cdot\mathbf{S}_3 \qquad (1)$$

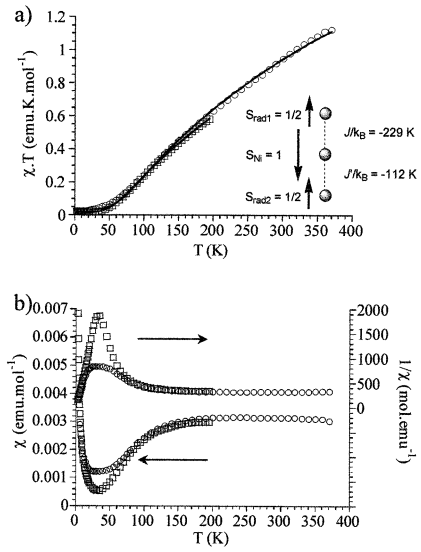


**Figure 9.** (a) Static $\chi\cdot T$ versus $T$ curve of compound **3**. First measure (□). Second measure (○). The solid lines represent the best fits. (b) Static $\chi$ versus $T$ (□) and $1\chi/$ versus $T$ (○) curves of compound **3**.

where $\mathbf{S}_1 = 1$, $\mathbf{S}_2 = \mathbf{S}_3 = ^1/_2$. Owing to the large radical−radical distance ($d >$ 4.0 Å), the $\mathbf{S}_2/\mathbf{S}_3$ interaction is fixed to zero. This Hamiltonian can be solved analytically, and the energy levels are spin multiplets characterized by the value of the total spin quantum number $\mathbf{S}_t$ ($\mathbf{S}_t = \mathbf{S}_1 + \mathbf{S}_2 + \mathbf{S}_3$). They are given by eqs 2−5:

$$E_1 = E(S_t = 0) = 2(J + J') \quad \text{(singlet)} \qquad (2)$$

$$E_2 = E(\alpha, \mathbf{S}_t = 1) = \frac{J + J'}{2} - \sqrt{X} \quad \text{(triplet)} \qquad (3)$$

$$E_3 = E(\beta, \mathbf{S}_t = 1) = \frac{J + J'}{2}\sqrt{X} \quad \text{(triplet)} \qquad (4)$$

$$E_4 = E(\mathbf{S}_t = 2) = -(J + J') \quad \text{(quintet)} \qquad (5)$$

$$\text{with } X = \left(\frac{J + J'}{2}\right)^2 + 2(J - J')^2$$

The molar susceptibility was derived from the usual expression (eq 6),[38] assuming $g_1 = g_2 = g_3 = g$.

$$\chi\cdot T = \left(\frac{Ng^2\mu_B^2}{3k_B}\right)\frac{\sum_{\mathbf{S}_t}\mathbf{S}_t(\mathbf{S}_t + 1)(2\mathbf{S}_t + 1)f(\mathbf{S}_t)}{\sum_{\mathbf{S}_t}(2\mathbf{S}_t + 1)f(\mathbf{S}_t)} \qquad (6)$$

$$\text{with } f(\mathbf{S}_t) = \sum_{\alpha}\exp\left[\frac{-E(\alpha,\mathbf{S}_t)}{k_B T}\right]$$

where $\alpha$ is used to index the various multiplets corresponding to the same $\mathbf{S}_t$ value.

(36) (a) Lange, C. W.; Conklin, B. J.; Pierpont, C. G. *Inorg. Chem.* **1994**, *33*, 1276. (b) Bruni, S.; Caneschi, A.; Cariati, F.; Delfs, C.; Dei, A.; Gatteschi, D. *J. Am. Chem. Soc.* **1994**, *116*, 1388.

(37) Stroh, C.; Turek, P.; Rabu, P.; Ziessel, R. *Inorg. Chem.* **2001**, *40*, 5334.

(38) (a) Belorizky, E. *J. Phys. I* **1993**, *3*, 423. (b) Belorizky, E.; Fries, P. H. *J Chim. Phys.* **1993**, *90*, 1077.

$$\chi \cdot T = \frac{1}{8} g^2 \left[ \frac{6(e^{-\Delta_1/T} + e^{-\Delta_2/T}) + 30e^{-\Delta_3/T}}{1 + 3(e^{-\Delta_1/T} + e^{-\Delta_2/T}) + 5e^{-\Delta_3/T}} \right] \quad (7)$$

$$\Delta_1 = \frac{1}{k}\left[ -\frac{3}{2}(J + J') - \sqrt{\left(\frac{J + J'}{2}\right)^2 + 2(J - J')^2} \right]$$

$$\Delta_2 = \frac{1}{k}\left[ -\frac{3}{2}(J + J') + \sqrt{\left(\frac{J + J'}{2}\right)^2 + 2(J - J')^2} \right]$$

$$\Delta_3 = \frac{1}{k}[-3(J + J')]$$

For complex **3**, the best fit with experiment was obtained with $g = 2.21$, $J/k_B = -230 \pm 25$ K, and $J'/k_B = -110 \pm 3$ K. As expected, very strong antiferromagnetic exchange interactions were found. A Curie tail, estimated to 2%, was also introduced to account for the large increase of $\chi$ at very low temperature. The use of a mean field interaction which would take into account intermolecular interactions does not notably improve the quality of the calculations. It is of interest to note that the use of a symmetric trimer model, where $J = J'$, gave a weaker exchange interaction but a significantly less satisfactory fit. Such a model is less appropriate due to the different orientations of both radicals toward the magnetic orbitals of the nickel center as shown by the crystal structure. Finally, it is assumed that the radical−radical interaction via the nickel center is very weak as found already for the zinc complex ($J_{rad-rad} < -5$ K), and that interaction via the saturated $CH_2-N-CH_2$ bridge is close to zero.

The EPR spectrum of the crystalline material at 100 K shows three signals, one at $g = 2.006$ attributed to the radicals and two additional signals at $g = 2.23$ and 2.04 due to the Ni(II) metal ion. In diluted acetonitrile solution, a weak five-line hyperfine pattern due to an isolated nitronyl-nitroxide radical is observed. Such a feature can be expected if the conformation in solution gives rise to decoupling of the radical with the nickel ion or by decoordination of one radical arm from the metal center. No other lines are observed, probably due to rapid relaxation processes.

It is usually assumed that Ni(II)−nitroxide complexes exhibit preferentially an antiferromagnetic exchange interaction.[39] However, in some specific cases, tailoring of the ligand induces ferromagnetic interactions due to coplanarity between the radical ring and the basal plane containing the metal.[40] This brings the $\pi^*$ SOMO orbital of the radical to be strictly orthogonal to the $d_{x^2-y^2}$ magnetic orbital of the metal, while its overlap with the $d_{z^2}$ is symmetry-forbidden.[41] In complex **3**, it is surmised that the prominent deviation from coplanarity is responsible for the very strong Ni−radical antiferromagnetic couplings likely due to a favorable magnetic orbital overlap (Scheme 3). The fact that both nitroxide fragments bind in equatorial positions is in keeping with strong antiferromagnetic interactions.

(39) Ulrich, G.; Stroh, C.; Ziessel, R. *C. R. Acad Sci.* **2001**, *4*, 113 and references therein.
(40) Luneau, D.; Romero, F. M.; Ziessel, R. *Inorg. Chem.* **1998**, *37*, 5078.
(41) Caneschi, A.; Gatteschi, D.; Renard, J.-P.; Rey, P.; Sessoli, R. *Inorg. Chem.* **1989**, *28*, 2940.

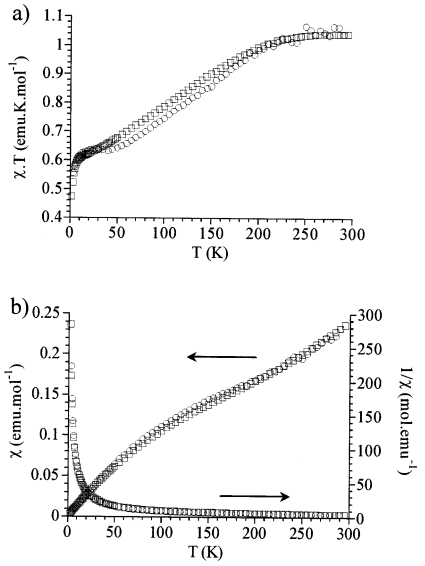


**Figure 10.** (a) Static $\chi \cdot T$ versus $T$ curve of compound **4**. First sample (○). Second sample (□). (b) Static $\chi$ versus $T$ (□) and $1/\chi$ versus $T$ (○) curves of compound **4**.

**Scheme 3**


**[Cu(bpyN(NIT)$_2$)](ClO$_4$)$_2$, 4.** Between room temperature and 250 K, this copper complex exhibits a constant $\chi \cdot T$ value of 1.1 emu·K·mol$^{-1}$ close to the expected value calculated for three independent $S = 1/2$ spins ($\chi \cdot T = 1.125$ emu·K·mol$^{-1}$). A sharp decrease of the moment is observed down to a plateau of 0.63 emu·K·mol$^{-1}$ at 40 K, followed by a further decrease below 20 K to a value of 0.55 emu·K·mol$^{-1}$ at 3 K (Figure 10a). Owing to this unusual magnetic behavior found for a copper(II) complex, similar measurements have been performed on a second sample prepared independently from a different batch of aminomethyl-bipyridine. These data are superimposable to the previous measurements and consequently exclude any artifacts or contamination from paramagnetic side products as seen in Figure 10. The $\chi$ versus $T$ curves show no maximum, and the reciprocal susceptibility versus temperature data deviate significantly from linearity (Figure 10b).

In light of the structural arrangement and magnetic behavior, different models could be suggested to understand the magnetic exchange pathways. First, it is quite obvious that a symmetrical or unsymmetrical linear trimer model could not be used. In fact, in the case of two NIT radicals with $g = 2.01$, $S = 1/2$, and a Cu(II) with $g = 2.2$, $S = 1/2$, where two spins are strongly antiferromagnetically coupled,

a resulting plateau at 0.454 emu·K·mol$^{-1}$ should be observed at low temperature. For example, this case has previously been found with the pincer type of ligands.[14] Here, the situation is clearly more complicated due to the fact that a plateau is found at 0.63 emu·K·mol$^{-1}$ and that many types of magnetic interactions have to be taken into account. More sophisticated models using discrete dimers connected in a different manner (six spin system)[38,42,43] were not adapted for the fitting sequence. One of them resulted in very high intermolecular ferromagnetic coupling between the radicals which is not realistic keeping in mind the large distances between these entities ($d$ > 3.70 Å) and the unfavorable orientation of the magnetic orbitals. The occurrence of higher clusters (larger than 3-spins) and/or of 3D networks is the only way to account for the observed plateau at 0.63·emu·K.mol$^{-1}$.

In order to have deeper insight in this unusual system, an EPR study was undertaken. Below 40 K, a polycrystalline sample of **4** shows a main resonance line at $g = 2.016$, and a half field signal at $g \approx 4.0$. At 140 K, a fine line appears, superimposed to the $\Delta M_s = \pm 1$ line (Figure 11a). By increasing the temperature, this signal increases, reaching a $g$ factor of 2.07. In parallel with the apparition of this peak, a sharp evolution of the peak to peak line width is observed. This observation could not be attributed to an axial to equatorial structure change as previously found in several copper complexes[44] but is most likely attributed to the flexibility of the axial NIT radical, which results in a less effective exchange interaction with the copper cation. This is also supported by the increase of the $g$ value by increasing the temperature (Figure 11b). Finally, the $I$·$T$ versus $T$ curve shows a plateau below ca. 50 K, in overall agreement with the observed behavior of the static susceptibility measured by SQUID.

Usually, the coupling between a copper and an axial nitroxide is ferromagnetic and of some tens of kelvins because of the weakness of the overlap density between the $d_{x^2-y^2}$ of the metal and the $\pi^*$ of the axial ligand, assuming that the axial ligand is situated on the O $z$ axis, and to the quite large distance between the radical and the metal center.[45] To confirm the well established dogma of weak ferromagnetic coupling when the radical is axially bonded, we have performed some modeling for our complexes. The magnetic orbitals (orbitals populated with one electron) calculated at the CASSCF level are depicted in Figure 12. The CAS comprises 3 electrons in the 3 magnetic orbitals. As expected, the first one is localized in the $d_{x^2-y^2}$ of the copper, the two other ones in the $\pi^*$ of the nitroxide radicals. However, results of the CASSCF calculation were not conclusive (we found two small ferromagnetic couplings),

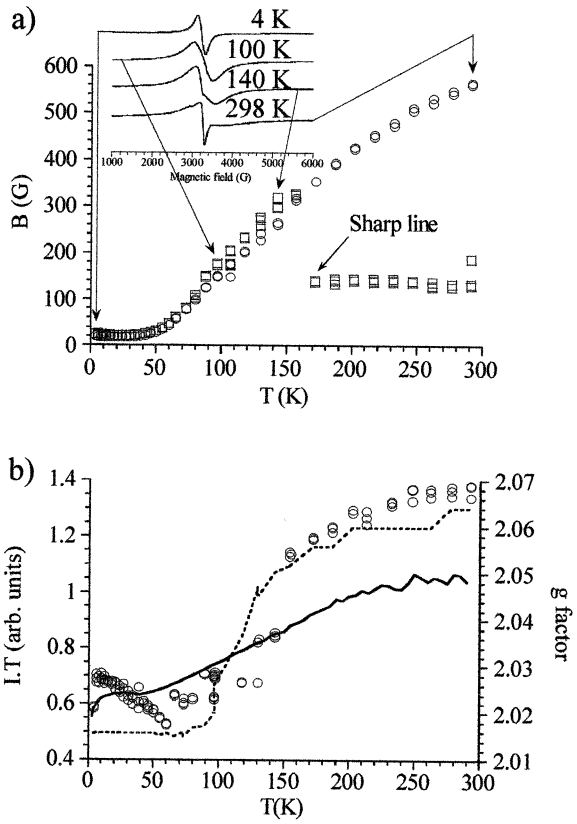


**Figure 11.** (a) EPR spectrum of crystalline Cu(II) complex **4**. Peak-to-peak (○) and half-height (□) broadness of the EPR spectra. (b) Normalized $I$·$T$ versus $T$ curve of compound **4** (○). The solid line corresponds to the static $\chi$·$T$ measure. The dotted line corresponds to the $g$ parameter variation.

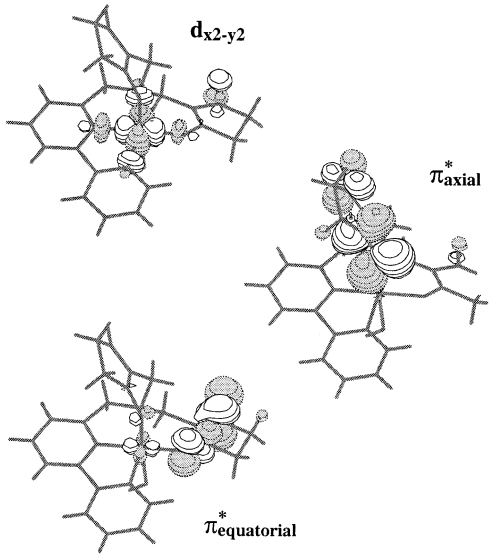


**Figure 12.** Density plots of the three magnetic orbitals of complex **4**.

and instead, to introduce more correlation, a simple analysis with EHT has been performed. The molecule is shared in three fragments: the podand, the copper atom, and the perchlorate. Overlaps between the molecular orbitals of these fragments are summarized in Table 5. Results for complex **3** have been added for comparison.

Although both overlaps are quite small, the $d_{x^2-y^2}$ of the copper overlaps better with the equatorial $\pi^*$ than with the axial $\pi^*$. It would confirm that ferromagnetic coupling could

(42) Belorizky, E.; Jeannin, M.; Rey, P. Rassat, A. *Solid State Commun.* **1993**, *85*, *735*.
(43) Fries, P. (University of Grenoble, and CEA Grenoble, France) supplied us with general software written by him, allowing the approximate resolution of spin systems up to eight with $S = {}^1/_2$ spins according to the general methods described in ref 38.
(44) Lanfranc de Panthou, F.; Belorizky, E.; Calemczuk, R.; Luneau, D.; Marcenat, C.; Ressouche, E.; Turek, P.; Rey, P. *J. Am. Chem. Soc.* **1995**, *117*, 11247.
(45) Di Matteo, A.; Barone, V. *J. Phys. Chem. A* **1999**, *103*, 7676.

**Table 5.** Overlap between the Molecular Orbitals of the Podand Fragment and the Atomic Orbitals of the Transition Metal Ion Calculated with EHT

| | **3** | | **4** | |
|---|---|---|---|---|
| | $\pi^*_1$ | $\pi^*_2$ | $\pi^*_{eq}$ | $\pi_{axial}$ |
| $d_{x^2-y^2}$ | 0.0007 | 0.0012 | 0.0065 | 0.0008 |
| $d_{z^2}$ | 0.0138 | 0.0147 | 0.0033 | 0.0048 |

**Table 6.** Comparison of the Geometrical Parameters and the Magnetic Couplings

| | **3** | | **4** | |
|---|---|---|---|---|
| | $\pi^*_1$[a] | $\pi^*_2$[b] | $\pi^*_{axial}$ | $\pi^*_{eq}$ |
| angle M−O−N (deg) | 119.7 | 121.5 | 110.0 | 119.0 |
| dihedral M−O−N−C (deg) | 36.5 | 28.4 | 0.0033 | 15.2 |
| distance M−O (Å) | 2.05 | 2.03 | 2.43 | 1.91 |
| $J$(K) | −230 | −110 | | |

[a] Belonging to the O3−N5 radical. [b] Belonging to the O5−N7 radical.

be effective with the axial radical, although the exchange parameters remain dramatically weak. The results for complex **3** are quite surprising: although the couplings for the two nitroxides are very different, the overlaps are similar. Geometrical parameters are summarized in Table 6. It is well-known that the dihedral angle M−O−N−C plays a key role in the overlap of the $\pi^*$ with the d orbitals of the metal,[23,46] and the closer it is to 90°, the larger is the overlap and the antiferromagnetic coupling. This agrees with our results despite the fact that we do not have a clear understanding of the couplings in complex **4**, but it seems that the radical in the equatorial position is strongly bonded to the copper with a very short distance of 1.91 Å resulting in a strong antiferromagnetic coupling as is usually the case in related compounds.[5,45]

## Concluding Remarks

Structural, magnetic, and electronic properties have been described for a series of complexes engineered from a podand-type of ligand bearing a central 6-aminomethyl-2,2′-bipyridine shaping unit linked via flexible spacers to nitronyl-nitroxide free radicals. Two types of structural arrangements have been found: (i) with Zn and Ni, the tertiary amine nitrogen and the two nitroxide oxygen atoms lie in a meridional conformation, while (ii) with Cu a facial conformation was found. This conformation accommodates the pronounced Jahn−Teller effect of copper and the fact that N donor atoms form particularly strong bonds owing to the presence of effective metal-to-ligand charge transfer interactions. The magnetic behavior of this copper complex is rather unusual and is dominated by strong antiferromagnetic interaction probably due to the radical located in the equatorial position. Despite many efforts, the global magnetic behavior could not parametrized with a simple magnetic interaction scheme. In the nickel case, the two coordinated radicals are strongly antiferromagnetically coupled to the metal in an asymmetric fashion with $J/k_B = -230 \pm 25$ K and $J'/k_B = -110 \pm 3$ K, due to a very efficient overlap between the SOMO orbitals of the radicals and the $d_{z^2}$ of the metal (Scheme 3). The values of these magnetic exchange interactions are certainly among the highest values reported for this kind of hybrid metal/radical system.[47] In the Zn case, a modest intramolecular interaction between both radicals of $J/k_B = -5.3 \pm 0.3$ K was found.

These novel complexes document the intimate relationship between magnetic properties and structural features and are typical examples of direct exchange, thereby enabling some conclusions to be made. The design of novel ligands is certainly interesting by itself, but the exact behavior during the complexation step such as the conformation, the angle between the magnetic orbitals, as well as the crystal packing of molecules is difficult to predict. However, the use of short spacers to link spin-labeled side arms is a way to constrain these subunits to adopt a noncoplanar conformation with the $d_{x^2-y^2}$ magnetic orbital, which is an ideal situation to obtain prominent magnetic couplings. Whereas this approach seems promising for high couplings, the prospects seem less brilliant concerning cooperative interactions, which is one of the key issues for the engineering of molecular magnets. We are now engaged in a program where the latter aspects are targeted with less sterically constrained scaffoldings.

**Acknowledgment.** This work was partially supported by the CNRS, and the ECPM. We would like to thank the referees for their valuable criticism of the manuscript and very interesting suggestions, and we are indebted to Dr. Paul Rey for fruitful discussions and some magnetic measurements. We also warmly thank Dr. Pierre Rabu and Dr. Marc Drillon from the IPCMS in Strasbourg (France), for helpful discussion concerning the parametrization of some of our magnetic measurements.

**Supporting Information Available:** Crystallographic data in CIF format. This material is available free of charge via the Internet at http://pubs.acs.org.

IC020484V

(46) Suaud, N.; Bolvin, H.; Daudey, J.-P. *Inorg. Chem.* **1999**, *38*, 6089.

(47) Ovcharenko, V. I.; Sagdeev, R. Z. *Russ. Chem. Rev.* **1999**, *68*, 345. 27.